2008 IEEE International Conference on
Robotics and Automation
Pasadena, CA, USA, May 19-23, 2008

Integrated Vision and Force Control in Suspended Cell Injection System: Towards Automatic Batch Biomanipulation

Haibo Huang, Dong Sun, James K. Mills, and Shuk Han Cheng

Abstract—**Automatic cell injection has been the focus of many researches and commercial development for several years. In this paper, a robotic cell injection system for automatic batch injection of suspended cells is developed. To facilitate the process, these suspended cells are held and fixed to a cell array by a specially designed cell holding device, and injected one by one through an "out-of-plane" cell injection process. A micropipette equipped with a PVDF micro force sensor is integrated in the proposed system. The force sensor is utilized to measure real time injection force applied to the cells during injection process. Through calibration of the relationship between the cell injection force and the desired injector pipette trajectory, a position (vision) and force control algorithm is proposed and applied to the motion control of the injection pipette in three-coordinate directions during an injection process. The out-of-plane cell injection task is decoupled into a position control in *X-Y* horizontal plane and an impedance force control in *Z*-axis. The depth motion of the injector pipette, a common problem of three-dimensional micromanipulation, is indirectly controlled by the force control. Finally, experimental results are given to demonstrate the effectiveness of the proposed approach.**

I. Introduction

Biological cell injection technology has played an important role in gene injection [1], in-vitro fertilization (IVF) [2], intracytoplasmic sperm injection (ISCI) [3] and drug development since it was invented. The cells to be injected in biological technology can be classified as adherent or suspended cells corresponding to two distinct biomanipulation tasks [4]. Currently, commercial devices such as those provided by Cellbiology Trading [5] are available for automation of adherent cell injection tasks. In contrast, development of methodologies for automatic injection of suspended cells has been the focus of a number of research groups [2, 6-7]. Traditional automatic suspended cell injection research as introduced in [7] is complex and time consuming. Unwanted suspended cell movement readily leads to the failure of this process. A number of potential solutions [8-9] have been proposed recently to solve the suspended cell injection problem with a method similar to that used in batch adherent cell manipulation. These methods attempt to fix suspended cells into arrays permitting batch cell injection to be performed.

Image-based visual servoing is the dominant control method in micromanipulation, but this approach has limitations in depth motion control due to the low depth of field, i.e. essentially planar image feedback. Furthermore, the control of injection forces is an important factor in the cell injection process. Current research approaches have begun to utilize force feedback in the cell injection process. Recent work in which a microinjection pipette has been bonded to the tip of a PVDF sensor to detect the injection forces in fish egg biomanipulation was performed in [10]. Sun *et al.* [11] developed a MEMS-based two-axis cellular force sensor to investigate the mechanical properties of mouse oocyte zona pellucida (ZP).

In this paper, a robotic cell injection system for automatic batch injection of suspended cells is proposed. A cell holding device is fixed on an actuated rotary plate, permitting suspended cells to be transported, one by one, into the injection site field of view. The injection process is achieved with the injector pipette tilted out of the focal plane of the microscope, as shown in Fig.1. It is essential to carry out the insertion with the micro-pipette held at an angle of attack with respect to the horizontal plane, in which the cells are held.

Furthermore, we develop a position (vision) and force control algorithm, where a micro-force sensor is mounted on injector pipette to measure real time injection force. First, a calibration of the cell membrane mechanical properties is performed with the injector pipette positioned in the same plane as the microscope focal plane, providing ideal injection geometry. Through a simple nonlinear regression, we derive an empirical relationship between the injection force and the desired cell injection trajectory. This allows us to infer a desired force input, based on out-of-plane injector depth measurements, obtained during cell injection. Then the out-of-plane cell injection task is decoupled into two relatively independent control processes: the position (vision) control in the horizontal (*X-Y*) plane and the force control in the depth direction (*Z*-axis). When the motion of the pipette in *X-Y* plane follows the desired cell injection trajectory utilizing visual feedback, the motion in the *Z*-axis, which cannot be observed under the microscope, is controlled

This work was supported by a grant from Research Grants Council of the Hong Kong Special Administrative Region, China [Reference No. CityU 119706], and a grant from City University of Hong Kong [Reference No. 7002127].

H. B. Huang and Dong Sun are with the Department of Manufacturing Engineering and Engineering Management, City University of Hong Kong, Kowloon, Hong Kong (e-mail: {hbhuang,medsun}@cityu.edu.hk).

J. K. Mills is with the Department of Mechanical and Industrial Engineering, University of Toronto, ON M5S 3G8 Canada (email: mills@mie.utoronto.ca).

S. H. Cheng is with the Department of Biology and Chemistry, City University of Hong Kong, Kowloon, Hong Kong (email: bhcheng@cityu.edu.hk).

indirectly through tracking the desired injection force. Based on the calibrated relationship between the injection force and the cell injection trajectory, the desired cell injection force can be deduced from the injector pipette motion as seen in the *X-Y* plane. With such a cooperation of vision and force control, the desired injection process can be achieved successfully.

II. System Design

2.1 System Setup

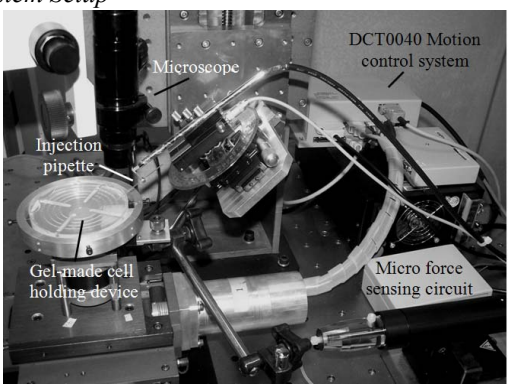

Fig. 1. A laboratory test-bed batch suspended cell injection system.

Fig. 1 illustrates an automatic suspended cell injection system developed in our laboratory. This system is designed to simulate automatic cell injection of large batches of suspended cells (such as zebrafish embryos) in biological engineering processes.

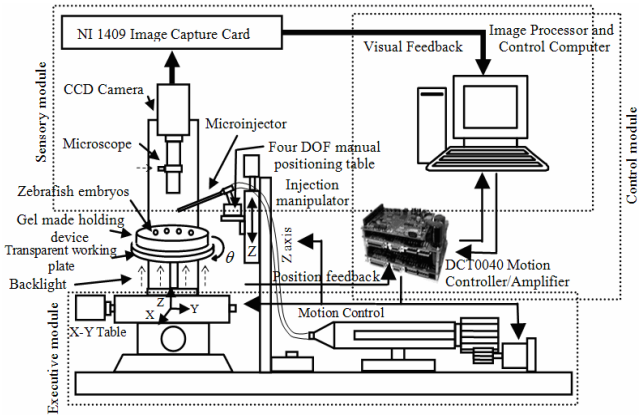

Fig. 2. Schematic of the cell injection system.

Fig. 2 illustrates a schematic of the system, which contains three modules. The executive module consists of an $X-Y-\theta$ positioning table with the injection mounted on the Z -axis. The cells to be injected are manually placed on a specially designed cell holding device, formed in a Petri dish, from agarose-gel, shown in Fig. 3. Mounted on the positioning table, the cell holder centre is coincident with the θ rotation axis. Coordinated motion of the $X-Y-\theta$ table and the Z -axis is required to perform the cell injection task. The pose of the injection pipette is precisely adjusted with a four degree of freedom (X - Y - φ - β) manual positioning table mounted on the *Z*-axis. The sensory module contains a vision system that includes an optical microscope, lighting system, CCD camera, PCI image capture and processing card, and image processing computer. The control module consists of a 2.8 GHz host computer and a DCT0040 motion control/drive system [12], with further details in [12-13].

2.2 Suspended Cell Holding Device

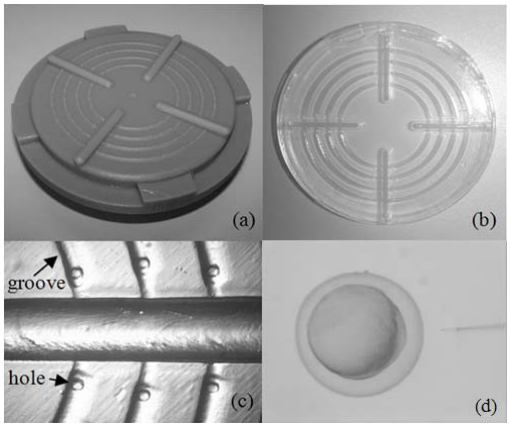

Fig. 3. Cell holding device. (a) mould; (b) agarose-gel made cell holder; (c) cell holding device under microscope; (d) zebrafish embryo placing in cell holder.

The proposed device for holding suspended cells in the system is shown in Fig. 3. Experiments shows that both the hemisphere hole shaped cell holder reported in [12] and the groove shaped cell holder reported in [9] have both advantages and disadvantages. The array of holes exhibits good capability to hold cells and significantly, the cells can be injected from all directions when they are positioned in this holder. However, placing cells in the individual holes is laborious work for batch injection. A far simpler and expedient approach is to place cells in the half-circle shape grooves. The injection direction is then restricted to along the radial direction of these grooves. Combining these two designs, a new prototype was fabricated in this research, as shown in Fig. 3. A holes array is embedded in a circular profile grooves which is centered about the geometric centre of the holder. Fig. 3(a) illustrates a cell holder mould which is fabricated using three-dimensional printing technology. The cell holding device is fabricated from low-melting point agarose gel, a material commonly used in biological research. To make this cell holding device, gel placed in Petri dish is made from 5% agarose by dissolving it in a microwave oven, and then a mould is pressed on the gel surface, and removed after agarose-gel has been cooled. Fig. 3(b) shows the agarose-gel cell holding device made by this mould and Fig. 3(c) is a local enlargement of Fig. 3(b) under microscope.

This design has three advantages. First, the grooves make positioning of cells more easily. Second, the holes array can immobilize the cells well and the cells will not move around and can be injected from all directions. Third, some fluid will be left in the grooves during the injection period and the image quality can be improved as shown in Fig 3. (d).

III. VISION AND FORCE INJECTION CONTROLLER

3.1 Cell Injection Control Strategy

During the out-of-plane cell injection, the depth motion of the injecting pipette cannot be observed by the microscope. We therefore propose to utilize a force control in the $Z-$ axis direction to implicitly control the depth motion. With an integration of a micro-force sensor feedback and vision feedback from the microscope, a hybrid vision and force control methodology is developed to control the interaction force between the pipette and the cell in the $Z-$ axis direction, and simultaneously control the motion of the pipette in the $X-Y$ plane. The control procedures are described as follows.

First, through a cell injection task calibration carried out in the $X-Y$ plane ($\varphi = 0$), i.e., injector pipette is positioned in the same plane as the microscope focal plane, the relationship between the cell biomembrane deformation and the cell injection force can be derived.

Assuming that batches of the same kind cells have the same membrane dynamic characteristics, similar injection force trajectory will be obtained for the same kind of cells when the injector pipette injects into the cells under the desired velocity and acceleration profile as reported in [14-15]. Through calibration experiments, an empirical relationship between, what will become the desired cell injection force F^d, and the desired injector pipette trajectory ρ^d can be obtained, i.e.

$$F^d = U(\rho^d) \tag{1}$$

With the use of a simply derived equation (1), obtained empirically, the desired injection force, corresponding to the desired position trajectory, can be estimated from the cell biomembrane deformation in the $X-Y$ plane and the known angle φ the injector pipette makes relative to the $X-Y$ plane. This desired injection force is the input to the force controller to be designed subsequently.

Second, the out-of-plane cell injection task can be decoupled into two relatively independent control process: the position (vision) control in horizontal ($X-Y$) plane and force control in depth (Z-axis). This idea attempts to control the position of the injector in $X-Y$ plane that can be observed, and simultaneously control the injection force using the force sensor in the Z-axis direction, in which depth information cannot be known. As indicated above, there exists an empirical relationship between the desired cell injection force and the desired cell injection trajectory. As a result, the depth movement of the injector can be indirectly controlled via force control.

Third, the out-of-plane cell injection control is implemented as follows. The movement of the pipette in the $X-Y$ plane is controlled using the computed-torque visual-based position control with injection force feedback. The purpose of this controller is to accurately control the injector pipette following the desired injection trajectory in the $X-Y$ plane. Then, based on the measured injector position in the $X-Y$ plane, inferring the actual position knowing the injector angle φ and the calibrated relationship between the injection trajectory and force, the desired injection force in the $Z-$ axis may be determined. Next, using the desired injection force in $Z-$ axis, an impedance force control algorithm is developed to control the injection force to follow the desired value and thus indirectly control the depth motion of the injector pipette.

3.2 Vision and Force Control in Cell Injection

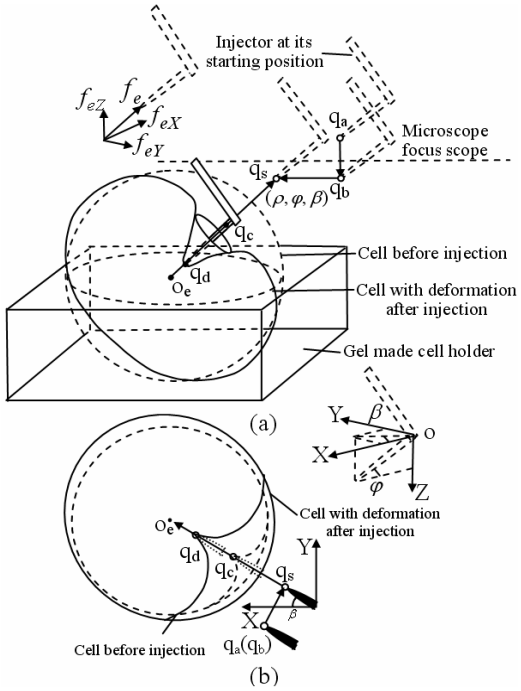

Fig. 4. Cell injection process and vision and force control design. (a) depth motion under force control; (b) planar motion under vision control.

A complete out-of-plane cell injection process with vision and force control is shown in Fig.4. The detailed batch biomanipulation process has been reported in [14-15]. During the cell injection process, the motion of the injector pipette can be simplified if the moving coordinate is presented in spherical polar coordinate frame. Define $o_e - \rho\varphi\beta$ as the spherical polar coordinate frame whose origin o_e is located at the center of the cell, as shown in Fig. 4, where β is the angle between the injector and the X - axis and φ is the tilt angle of the injector. The desired trajectory of the injector pipette can be expressed as

$$q^d_{XYZ} = \begin{bmatrix} X^d \\ Y^d \\ Z^d \end{bmatrix} = \begin{bmatrix} \rho^d \sin\varphi\cos\beta \\ \rho^d \sin\varphi\sin\beta \\ \rho^d \cos\varphi \end{bmatrix} \tag{2}$$

where both angles β and φ do not change during the cell injection process.

The dynamics equation during the injection process in orthogonal coordinates can be partitioned into two distinct equations of motion, namely

$$\begin{cases} \tau_{XY} = M_{XY}\ddot{q}_{XY} + N_{XY}\dot{q}_{XY} + J^T f_{eXY} \\ \tau_Z = M_Z\ddot{Z} + N_Z\dot{Z} + G_Z + J^T f_{eZ} \end{cases} \tag{3}$$

where τ_{XY} is a 2×1 vector corresponding to the torque in $X-Y$ plane, M_{XY} and N_{XY} are sub-matrices of M and N corresponding to the X, Y axes, M_Z, N_Z and G_Z are sub-matrices of M, N and G corresponding to the Z axis, and f_{eXY} and f_{eZ} are the actual injection forces in $X-Y$ plane and Z axes measured from PVDF micro force sensor.

Define the desired injector trajectory as q_{XY}^d. Tracking of this trajectory in $X-Y$ plane can be ensured by using a computed torque controller with measured injection force compensation, i.e.,

$$\tau_{XY} = M_{XY}(\ddot{q}_{XY}^d + k_{v1}\dot{e}_{XY} + k_{p1}e_{XY}) + N_{XY}\dot{q}_{XY} + J^T f_{eXY} \quad (4)$$

where $q_{XY}^d = \rho^d \sin\varphi \begin{bmatrix}\cos\theta \\ \sin\theta\end{bmatrix}$, $e_{XY} = \rho^d \sin\varphi \begin{bmatrix}\cos\theta \\ \sin\theta\end{bmatrix} - \begin{bmatrix}X \\ Y\end{bmatrix}$ is the position error in the $X-Y$ plane, k_{v1} and k_{p1} are position and velocity gain matrices. The controller (4) leads to a closed loop equation of $\ddot{e}_{XY} + k_{v1}\dot{e}_{XY} + k_{p1}e_{XY} = 0$, which implies $e_{XY} = 0$.

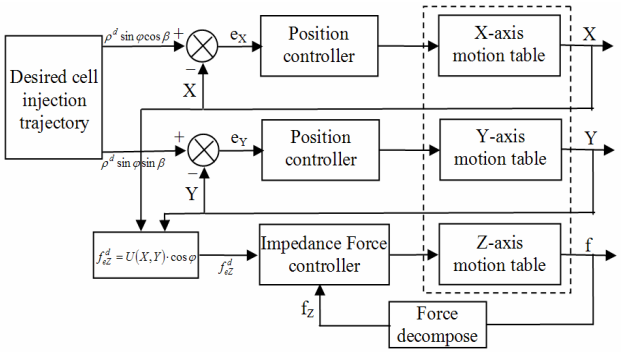

Fig. 5. Vision and force control block diagram.

As for the depth movement of the injector, an impedance force control algorithm is utilized to control the injection force to follow the desired injection force, which indirectly controls the position of the injector in $Z-$axis.

The contact space impedance force control is given as:

$$m\ddot{e}_Z + b\dot{e}_Z + ke_Z = f_{eZ} \quad (5)$$

where m, b and k are the desired impedance parameters, $e_z = Z^d - Z = \rho^d\cos\varphi - Z$, representing the position errors of the injector in $Z-$axis, ρ^d denotes the desired injector pipette trajectory. The actual position Z can be obtained from the encoder of motor.

We now solve for $\ddot{Z}$ from equation (5) and substituting it into (3) yields a $Z-$axis torque controller as follows:

$$\tau_Z = M_Z\left(\ddot{Z}^d + m^{-1}\left(b\dot{e}_Z + ke_Z - f_{eZ}\right)\right) + N_Z\dot{Z} + G_Z + J^T f_{eZ}^d \quad (6)$$

where $f_{eZ}^d = U(X,Y)\cos\varphi$ denotes the desired injection force, which can be obtained from the injector position in the $X-Y$ plane and the calibrated relationship between the injection trajectory and force.

Substituting (6) into (3) leads to a closed-loop equation:

$$M_Z m^{-1}\left(m\ddot{e}_Z + b\dot{e}_Z + ke_Z - f_{eZ}\right) = J^T\left(f_{eZ} - f_{eZ}^d\right) \quad (7)$$

Substituting (5) into (7) leads to $f_{eZ} = f_{eZ}^d$, then $f_e = f_e^d$. The block diagram of this vision and force control is shown in Fig. 5.

IV. Experiments

To verify the effectiveness of the proposed approach, experiments were performed on the setup, a shown in Fig. 1 and more details introduced in Section II. For simplicity, the rotation angle between the image frame and the stage frame is set to zero ($\alpha = 0^\circ$). The displacement between origins of the two frames is $d = [0,\ 0,\ 30mm]^T$. The magnification factor of the microscope objective is $\lambda = 30$. The dynamic model inertia and damping matrices, and gravitational force vector have been estimated with their values reported in [14-15]. The angles between the injector pipette and the X- and Z-axis axis are $\beta = 45^\circ$ and $\varphi = 35.26^\circ$, respectively.

The cells selected for injection were Zebrafish embryos, which are commonly chosen as an animal model in biomanipulation. The diameter of the Zebrafish egg is approximately 1.15-1.25 mm (including chorion). The radius of the injector pipette is $c = 7.5\mu$m.

4.1 Force Calibration

Calibration experiments were performed to obtain an empirical relationship between the desired cell injection force F^d and the desired injector pipette trajectory ρ^d. To achieve this goal, we measured the cell injection force using the PVDF micro force sensor while recording the desired injector pipette trajectory ρ^d. To obtain consistent calibration results, calibration tests used identical radius of the pipette, and identical velocity and acceleration profiles, as in the out-of-plane cell injection. During the pre-piercing period $(0\,\text{sec} < t < 0.5\,\text{sec})$, the injector was accelerated to move a distance of 317.5 μm to reach the maximum velocity of 1270 $\mu m/s$ when it contacted the cell membrane. During the next piercing period $(0.5\,\text{sec} < t < 1\,\text{sec})$, the pipette was decelerated and pierced the cell membrane, moving 317.5 μm within the cell. Then, it took about 2 seconds to inject the genetic materials into the cell. Finally, the injector pipette was extracted from the cell $(3.00\,\text{sec} < t < 5.23\,\text{sec})$, using lower speed than during the piercing period, where the maximum velocity was 635 $\mu m/s$.

A number of embryos were used in these calibration experiments. Fig. 6 illustrates three typical results obtained in planar cell injection experiments. Note that the force threshold for penetration of the cell membrane differs from embryo to embryo due to variation of cell properties. This difference in penetration forces is not problematic as the micro force sensor is sensitive to the sudden large force changes as the micro-pipette penetrates the cell. The averages of these forces are plotted in Fig. 7. Through curve fitting, the relationship between the cell injection force and the desired

injector pipette trajectory ρ^d, the injection force F was estimated by the following equation:

$$F = 0.0001694 \cdot (r - \rho^d)^2 + 0.3987 \cdot (r - \rho^d) - 8.389 \qquad (8)$$
$$r > \rho^d > r - 317.5\mu m$$

where r is the radius of injected cells.

This force-position curve will be subsequently used to guide the insertion of the injector pipette. The process is to move X and Y axes simultaneously according to the desired injector pipette trajectory ρ^d, and then based on the actual X and Y to determine the desired injection force at the time instant for $Z-$ axis force control. During the pre-piercing period, the micro force sensor is used to detect whether the pipette and the embryo get contact. When the contact is confirmed, the controller switches to the position(vision) and force controller as shown in Fig. 5.

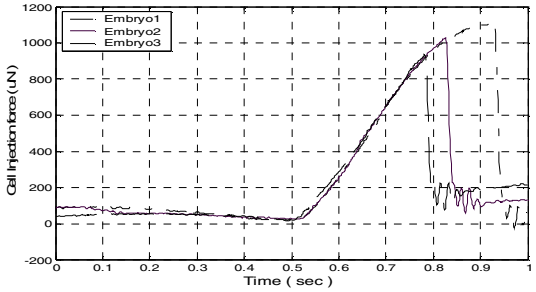

Fig. 6. Cell injection force calibration.

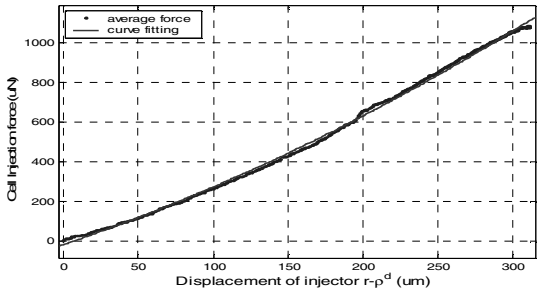

Fig. 7. Curve fitting result of desired force.

4.2 Experimental Results

In all injection experiments, although each test used a different embryo cell, the mechanical properties of all cell biomembranes are uniform since they were all collected in accordance with the standard embryo preparation procedures, and all were injected after being placed at room temperature ($22^\circ C$-$24^\circ C$) for 2 hours after fertilization (blastula stage). During the pre-piercing period, the computed torque control gains were $k_{v1} = diag\{21.645,\ 28.87,\ 31.75\} \times 10^3 s^{-1}$, $k_{p1} = diag\{27.42,\ 43.4,\ 66.4\} \times 10^6 s^{-2}$. During the piercing period, the controller switched to the proposed hybrid position(vision) and force controller (4) and (7), where the computed torque control gains were the same as the above, and the impedance control gains were $m = diag\{0.330,\ 0.165,\ 0.1635\} N \cdot s^2/m$, $b = diag\{7.143,\ 4.763,\ 5.191\} \times 10^3 N \cdot s/m$, $k = diag\{9.049,\ 7.144,\ 10.855\} \times 10^6 N/m$. Experimental results for one of the injected embryo cells, during the piercing period of the injection process ($0\,\text{sec} < t < 1\,\text{sec}$), are provided below.

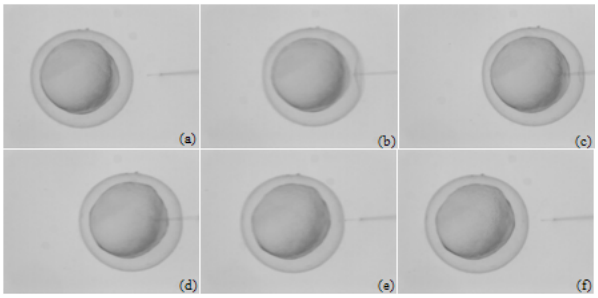

Fig. 8. An out-of-plane cell injection process with vision and force control.

An entire out-of-plane injection process with vision and force control is shown in Fig. 8. A glass injector reaches its starting position in (a), and contacts the biomembrane of cell in (b). The pipette pierces into the cell in (c), then pulled out of the cell in (d) and (e), and back to the starting point in (f).

Fig. 9 illustrates position tracking results in $X-$ axis (a) and $Y-$ axis (b) respectively. It is seen that the actual position could follow the desired position very well, and the maximum position tracking error in each axis was around 1.5 μm. This demonstrates that the vision (position) control based on the computed torque control strategy exhibits satisfied tracking performance for such a micro manipulation.

Fig. 10 illustrates the injection force control results in $Z-$ axis, and the depth motion error that was indirectly controlled via force control. During the pre-piercing period ($0\,\text{sec} < t < 0.5\,\text{sec}$), the injection force was zero. When the injector pipette contacted the cell after injection started for 0.5 second, the force control was implemented and appeared to be effective to ensure the actual injection force to follow the desired one. The maximum force error along $Z-$ axis was around 60 μN. The maximum position error in $Z-$ axis was around 6 μm, which was relatively large compared to that in $X-Y$ plane. Since the depth motion cannot be observed from microscope, it can only be controlled indirectly through the force control. This explains why $Z-$ axis position accuracy is worse than in the $X-Y$ plane. Nevertheless, the error of 6 μm is still within a satisfactory range.

Fig. 11 illustrates both position and force tracking errors after combining the results in $X-$, $Y-$ and $Z-$ axes. This position error denotes the difference between each actual position in 3D space and the desired position calculated by the desired pipette trajectory ρ^d and the fixed angles β and φ. The force error was detected along the pipette axis by the installed PVDF force sensor. It is seen that the maximum position error corresponds to the maximum force error. This is because that the depth control follows the force control in $Z-$ axis, and the force control performance has great influence on the depth control and hence the whole position control performance.

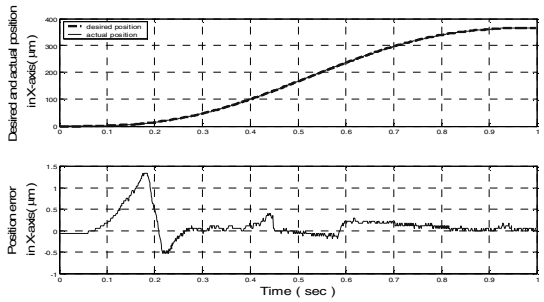

(a) Position tracking results in X-axis

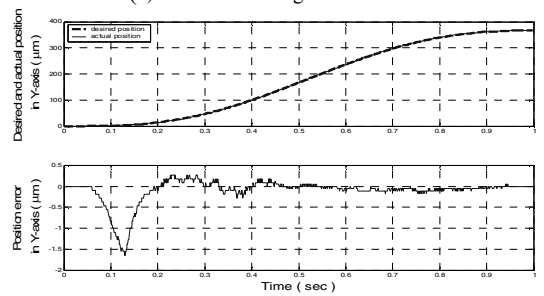

(b) Position tracking results in Y-axis

Fig. 9. Position tracking results in X-Y plane.

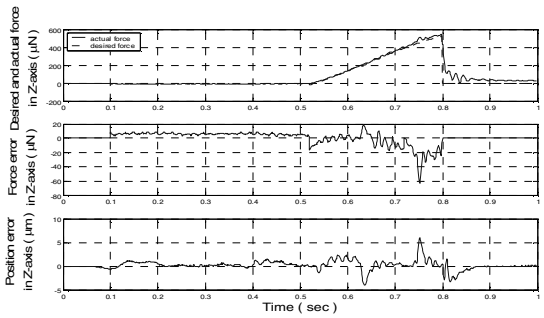

Fig. 10. Injection force control results in Z- axis and depth motion error.

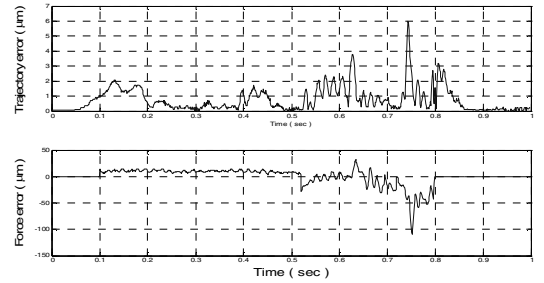

Fig. 11. Combined position and force tracking errors.

TABLE I. EVALUATION OF CONTROL PERFORMANCE

Max errors	Embryo 1	Embryo 2	Embryo 3	Embryo 4	Embryo 5	Mean error
Force (μN)	109	120	110	112	130	116.2
Position (μm)	6	7	10	9	11	8.6

The same experiment was repeated twenty times to simulate out-of-plane cell injection of a batch (20) of zebrafish embryos. Table I shows the maximum force and position errors of five randomly selected embryos. It is clear to see that the proposed control method exhibits stable and uniform performance in out-of-plane cell injection of a batch of Zebrafish embryos.

V. CONCLUSION

In this paper, a new robotic biomanipulation system for automatic injection of batches of suspended cells is developed. A cell holding device, fixed on the rotary plate, permits cells to be transported, one by one, into the injection field of view. A position (vision) and force control algorithm is developed and applied to motion control of the injection pipette in three-coordinate directions during out-of-plane cell injection process. The out-of-plane cell injection task is decoupled into a horizontal plane position control and an impedance force control in Z -axis. The depth control of the injector pipette in Z -axis, which is a common problem of many three-dimensional micromanipulation, can be indirectly realized by the force control. Finally, the effectiveness of the proposed approach is demonstrated experimentally.

REFERENCES

[1] J. Kuncova and P. Kallio, "Challenges in Capillary Pressure Microinjection", Proc. IEEE Int. Conf. of EMBS, pp. 4998-5001, 2004.

[2] Y. Sun and B.J. Nelson, "Biological cell injection using an autonomous microrobotics system," The Int. Journal of Robotics Research, vol. 21, pp. 861-868, 2002.

[3] K. K. Tan, D. C. Ng and Y. Xie, "Optical intra-cytoplasmic sperm injection with a piezo micromanipulator," The 4th World Congress on Intelligent Control and Automation, pp. 1120-1123, 2002.

[4] Pasi Kallio and Johana Kuncova, "Manipulation of Living Biological Cells: Challenges in Automation," presented at the workshop on Microrobotics for Biomanipulation in the Int. Conf. on Intelligent Robots and Systems, IROS'03, Las Vegas, USA, 2003.

[5] http://www.ais2.com.

[6] M. Ammi and A. Ferreira, "Realistic visual and haptic rendering for biological-cell injection," Proc. IEEE Int. Conf. on Robotics and Automation, pp.918-923, 2005.

[7] X. D. Li, G. Zong and S. Bi, "Development of Global Vision System for Biological Automatic Micro-Manipulation System," Proceedings of the IEEE Int. Conf. on Robotics and Automation, Vol.1, pp. 127-132, 2001.

[8] X. J. Zhang, Matthew P. Scott and Calvin F. Quate, etc. "Microoptical Characterization of Piezoelectric Vibratory Microinjections in Drosophila Embryos for Genome-Wide RNAi Screen," Journal of Microelectromechanical Systems, Vol.15, No. 2, pp. 1-10, 2006.

[9] Z. Lu, Peter C Y Chen and J. Nam, etc., "A micromanipulation system with dynamic force-feedback for automatic batch microinjection," Journal of Micromechanics and Microengineering, Vol. 17, pp. 314-321, 2007.

[10] D. H. Kim, S. Yun and B. Kim, "Mechanical force sensor response of single living cells using a microrobotic system," Proc. IEEE Int. Conf. on Robotics and Automation, pp. 5013-5018, 2004.

[11] Y. Sun, K. T. Wan and K. P. Roberts, etc., "Mechanical property characterization of mouse zona pellucida," IEEE/ASME Transactions on Nanobioscience, vol. 2, pp. 279-286, 2003.

[12] T. Fujisato, S. Abe and T. Tsuji, etc., " The development of an OVA holding device made of microporous glass plate for genetic engineering," Proceedings of the 20th Annual Int. Conf. of the IEEE Engineering in Medicine and Biology Society, vol. 20, pp. 2981-2982, 1998.

[13] http://www.dynacitytech.com.

[14] H. B. Huang, D. Sun, J. K. Mills, and W. J. Li, "Visual-based impedance force control of three-dimensional cell injections system," Proc. IEEE Int. Conf. on Robotics & Automation, pp. 4196-4201, 2007.

[15] H. B. Huang, D. Sun, J. K. Mills, and W. J. Li, "Visual-based impedance control of out-of-plane cell injection systems," IEEE Trans. on Automation Science and Engineering, conditionally accepted, 2007.